BrainSim: AI-Driven Brain MRI Simulation for Alzheimer's Disease Diagnosis

Yueyi Bao *

The Hill School, 860 Beech St, Pottstown, PA, USA

* Corresponding Author Email: yvonnebao0620@gmail.com

Abstract. Alzheimer's Disease, a progressive neurodegenerative disorder with no cure, presents a formidable challenge to global healthcare. The simulation of brain states, encompassing both rejuvenation and aging, aids clinicians in understanding disease progression and early detection. Recent advances in deep adversarial neural networks, effective in generating age-varied facial images, are now applied to brain MRI simulations across different time states. However, existing methods for brain MRI synthesis predominantly focus on aging simulation, lacking rejuvenation capabilities, and relying heavily on longitudinal data. Access to rejuvenated brain scans is essential as it can help researchers track the structural changes and biomarkers in the early stage of AD, facilitating AD research and personalized treatments. Additionally, previous methods are often 2D-based, failing to capture complex 3D spatial information obtained by 3D scans. To overcome these limitations, I propose BrainSim, a novel longitudinal brain MRI synthesis framework. Specifically, BrainSim leverages a bidirectional cycle-consistent generative neural network to generate rejuvenated and aged MRI scans simultaneously using cross-sectional scans only. BrainSim incorporates a 3D conditional U-Net as its fundamental model, facilitating the direct generation of 3D MRI scans conditioned on the subject's health state and sex. BrainSim was evaluated against benchmark models using longitudinal data and a pre-trained age predictor to assess the quality of generated images. Experiments using the ADNI dataset show BrainSim's state-of-the-art performance in brain aging and rejuvenation tasks, marking significant advancements in MRI synthesis for Alzheimer's research and drug development.

Keywords: Alzheimer's Disease, Generative Adversarial Network, Magnetic Resonance Imaging, Brain Aging and Rejuvenation.

1. Introduction

Alzheimer's disease (AD) is the most common age-related neurodegenerative disorder [1]. However, the underlying mechanism has not been completely revealed, and adverse effects accompany the existing treatments and the response is limited [2].

Past studies have shown that a diagnosis early in the course of illness allows time for all concerned to adjust whilst the patient can still actively engage, and offers access to both non-pharmacological and pharmacological treatments. Many patients with mild-to-moderate Alzheimer's dementia can live with the disease for several years with a good quality of life and access to the optimal treatments and resources [3]. Therefore, alternative diagnosis of AD requires urgent development. Prior research has suggested that accurate simulations of the brain's chronicle-changing process can provide prognostic information about the progression of individuals to cognitive decline, dementia, and subsequent death [4]. Brain imaging is also helpful in improving the biological classification of AD by allowing proposed classifications based on pathology to be applied in vivo, opening a new window of therapeutic intervention at preclinical stages [5].

Brain MRI Imaging is a well-established tool for AD diagnosis [6]. Specifically, longitudinal MRI studies are helpful in the process of AD research and diagnosis as they can capture the aging process of individuals, allowing researchers to investigate individual variability by testing the interaction of between- and within-subject effects. However, longitudinal studies must include multiple time points, covering the specific life period under investigation in each subject. This nature of longitudinal MRI studies thus makes them notoriously difficult to perform in humans. For pragmatic reasons, they can suffer from an important drop-out of participants and usually cover a short period of subjects' lives

(usually less than 10 years) [7], [8], [9]. Moreover, consistent longitudinal MRI scans are difficult to acquire due to the inconsistent longitudinal scans among subjects and the heterogeneous progressions of high-dimensional regions of interest (ROIs) in MRI. Even in ADNI [10], one of the most well-known large-scale datasets, longitudinal images are acquired at a few time points and cover only a few years.

Many non-deep learning models were used for MRI image synthesis. Hajij et al. proposed an MRI synthesizer based on Normalizing Flows, an approach that transforms unknown complex distributions into simpler ones [11]. The penalized likelihood model was used by Pal et al. to generate personalized MRI images [12]. Researchers reported that the performance of these models provides a promising indication of non-deep-learning models' capability in medical image generation [11].

On the other hand, deep learning based methods are more prevalent nowadays. They have been employed to forecast the future degeneration of human brains by leveraging existing scans [13], [14]. Researchers have found that compared to conventional methods, deep learning-based methods demonstrate superior performance in generating more realistic synthetic images with higher similarity to real images and better quantitative metrics [15]. Xia et al. proposed a deep learning-based method that learns to simulate subject-specific brain aging trajectories without relying on longitudinal data [13]. Despite its significant improvements from the previous approaches, however, this simulator is also constrained by two limitations. As a one-directional generative adversarial network, the proposed model fails to achieve brain rejuvenation. Past studies have shown that brain rejuvenation has equal importance as brain aging to provide valuable information about AD progression and diagnosis. In addition, this method, along with many other previous simulators, is limited to the simulation of 2D MRI slices and can only generate MRI scans slice-by-slice. Thus, these existing models fail to capture the complex 3D spatial relationships among brain structures inherent in 3D MRI scans.

Here, I propose BrainSim to address the limitations identified from existing models. BrainSim is a bidirectional CycleGAN network that is capable of synthesizing 3D retrospective and aged brain MRI scans for a desired age, sex, and health state. In this paper, I build a deep learning-based model that can be trained without longitudinal data. A simplified schematic of BrainSim is shown in Fig. 1. Given a brain image, BrainSim produces a brain of the same subject at the target ages. The input image, divided into one of the two domains depending on the need, is first encoded into a latent space, which is modulated by two vectors representing the age difference and health state (AD, MCI, and CN), respectively. The conditioned latent space is finally decoded into an output image (the synthesized aged and/or retrospective image). Based on the CycleGAN framework, the proposed model has two sets of Generators and Discriminators that are trained to either learn the joint distribution of brain appearance, age, sex, and health state or encourage accurate synthesis of MRI scans at the desired age. Multiple loss functions are also purposed to maintain the subject identity and accuracy of the generated images.

BrainSim was trained and tested using the ADNI dataset and evaluated using both quantitative and qualitative metrics. I pre-trained an AI-based age predictor and used the age estimation as a proxy metric for age accuracy. I also show qualitative results by performing aging and rejuvenating simulations on different health states and conducting longitudinal image synthesis. Both quantitative and qualitative results show that BrainSim outperforms benchmarks with more accurate simulations that capture the characteristics specific to each individual in different health states.

My contributions are summarized as follows:

- Proposed a bidirectional CycleGAN network to simulate both the brain's aging and rejuvenating process and perform subject-specific brain aging synthesis, trained on cross-sectional data overcoming the need for longitudinal data.
- Designed a 3D conditional U-Net that generates 3D MRI scans that can maximize the preservation of details regarding the morphological structure of the brain.
- Incorporated sex as a factor for image generation and discrimination to encourage sex-specific structural changes in the synthesized image.

2. Method

In this section, I first introduce the structures of data involved and the data processing workflow. Then, I introduce the architecture of the proposed model, BrainSim.

2.1. BrainSim Framework

The proposed BrainSim, built on Zhu et al.'s CycleGAN model, features a framework comprising two generator networks (G_X and G_Y) and two discriminator networks (D_X and D_Y), as shown in Figure 1. G_X generates aged 3D brain scans $G_X(X_{yng})$ from the younger-age brain X_{yng}, while G_Y producing retrospective scans $G_Y(Y_{old})$ from older-age brain Y_{yng}, both aiming to deceive the discriminators. Notably, X_{yng} and Y_{old} are scans from distinct individuals, with Y_{old} being older than X_{yng}. Additionally, the synthetic brain image $G_x(X_{yng})$ and $G_Y(Y_{old})$ should retain the subject identity, i.e. belong to the same subject as the input X_{yng} and Y_{old}, throughout the aging and rejuvenating process. D_X and D_Y are tasked with distinguishing between these generated scans and authentic brain images.

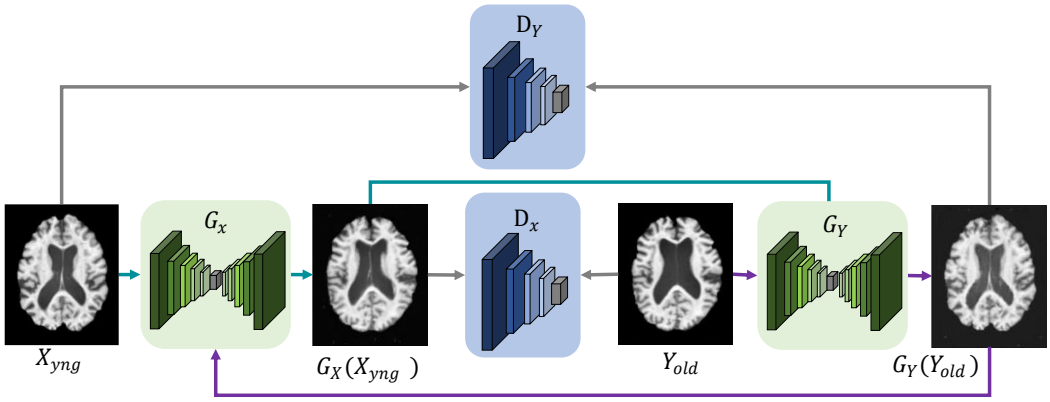

Figure 1. Overview of the proposed BrainSim model

$G_x(X_{yng})$ and $G_Y(Y_{old})$ are the output (aged and retrospective, respectively) image from domain X (supposedly belonging to the same subject of X_{yng} and Y_{old}) of the target age and health state. The Generator G_x / $G_Y$takes as input X_{yng}/Y_{old}, and outputs $G_x(X_{yng})/G_Y(Y_{old})$; the Discriminator takes as input a generated brain image and a ground truth, and outputs a discrimination score.

The contributions of my approach, shown in Fig. 1, are the design of the conditioning mechanism and the 3D bidirectional CycleGAN network. I detail all these below.

2.1.1. Conditioning on Age and Health State

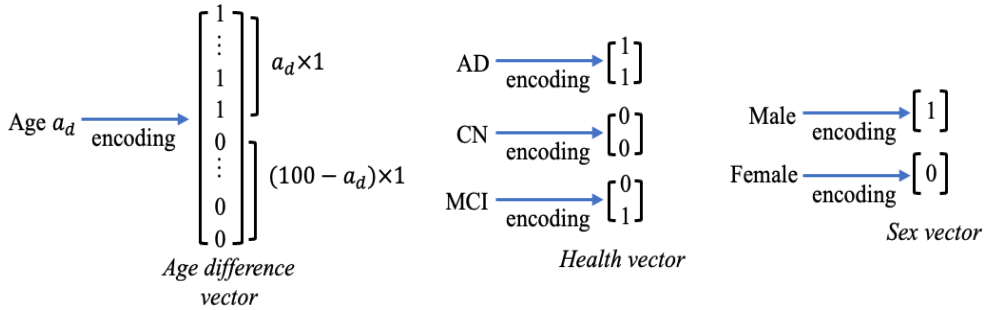

Figure 2. Ordinal encoding of age difference and health state

The Left shows how I represent age difference using a binary vector with the first a_d elements as 1 and the rest as 0; the middle is the encoding of health states, I used a 2 × 1 vector to represent three categories of AD status; the right is the encoding of sex of the patients, I used a 1x1 vector ([0] for female; [1] for male).

In the proposed BrainSim model, I used ordinary binary vectors to encode the health state, sex, and age of the subjects, which are embedded in the bottleneck layer of the Generator. I used a 2×1 vector to encode the health state and a 1×1 to encode the patient's sex. Similarly, I used a 100×1 vector to encode the designated age difference, assuming a maximum difference of 100 years. A simple illustration of this encode is illustrated in Figure 2.

2.1.2. Generator

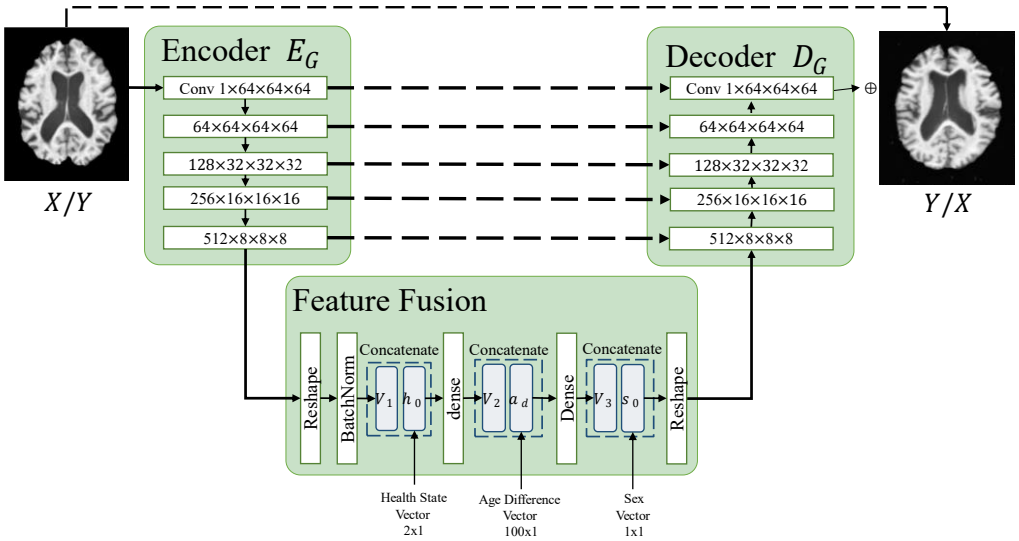

Figure 3. Detailed architecture of the conditional U-Net Generator

The Generator contains an encoder E_G to extract latent features, a feature fusion module to incorporate the target age and health state into the latent features to involve the target age and health state, and a decoder D_G to generate aged and retrospective images.

The generator G takes as input 3D brain images X_{yng} and Y_{old}, and ordinal binary vectors for target health state h_0 and age difference a_d. The age difference vector is conditioned to $a_d = |a_X - a_Y|$, such that the generator G_x generates an image that is a_d years older than that of X_{yng}, while Generator G_Y generates an image that is a_d years younger than that of Y_{old}.

G has three components, Encoder E_G, gesture fusion module F_G, and Decoder D_G. E_G extracts latent features from the input images while F_G fuses the target age and health state into the network. Lastly, D_G generates the aged/retrospective brain image from the bottleneck features. To incorporate age and health state information into the model, I start by combining the latent vector V_1, derived from E_G, with the health state vector h_o. Next, this merged vector undergoes processing to produce the latent vector V_2, which is concatenated with the difference age vector a_d. Finally, the resulting vector V_3 is concatenated with the sex vector s_0, utilized to generate the output image. I adopted long-skip connections between layers E_G and D_G to preserve input image details and enhance the sharpness of the output images [26]. In summary, the Generator's forward pass can be expressed as:

$G_X(X_{yng}) = G_X(X_{yng}, a_d, h_0, s_0)$ and $G_Y(Y_{old}) = G_Y(Y_{old}, a_d, h_0, s_0)$.

2.1.3. Discriminator

The Discriminator implemented is a Multi-Layer Discriminator. The discriminator architecture consists of multiple layers of convolutional neural network followed by activation functions such as ReLU (Rectified Linear Unit) and leaky ReLU, a type of activation function based on a ReLU [27].

The discriminator is made up of 3 convolutional neural networks, with each layer in the discriminator extracting features from the input data and learning increasingly abstract representations as the data flows through the network. Between the three layers, the dimension of the image is transformed from (64, 64, 64) to (4, 4, 4), with a channel number of 512. The discriminator can capture complex patterns and features in the data, allowing it to better discriminate between real and fake samples.

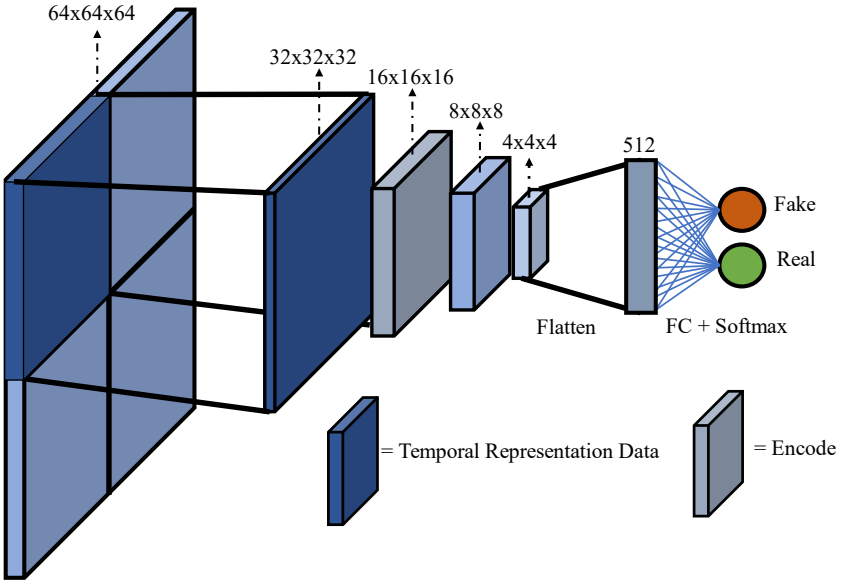

Figure 4. Detailed architecture of the Multi-layer Discriminator

The discriminator consists of 3 layers, Each layer extracts increasingly abstract features from the input data. The real and fake sample generated by the generator is distinguished after the feature abstraction process.

The final layer uses a sigmoid activation function to squash the output into the scalar vector between [0, 1], where values close to 1 represent real images and values close to 0 represent fake images.

2.2. Loss Functions

BrainSim is trained with a multi-component loss function containing adversarial, cycle-consistent, and identity-preservation losses.

(a) *Adversarial Losses*: The adversarial loss aims to measure the discriminability between aged or retrospective brain images with the ground truth, pushing the generator towards authentic outputs. The loss function is given by:

$$\mathcal{L}_{adv_X}(G_X, D_X) = \mathbb{E}_{y\sim p(Y_{old})}[D_X(G_X(y))] - \mathbb{E}_{x\sim p(X_{yng})}[D_X(x)]$$

Where the differences between the retrospective image $G_X(y)$ is compared to the ground truth image X. Similarly, for G_Y and D_Y:

$$\mathcal{L}_{adv_Y}(G_Y, D_Y) = \mathbb{E}_{x\sim p(X_{yng})}[D_Y(G_Y(x))] - \mathbb{E}_{y\sim p(Y_{old})}[D_Y(y)]$$

The optimization process of G_X and D_X is:

$$\min_{G_X}\max_{D_X}\mathcal{L}_{advX}(G_X, D_X)$$

Similarly, the optimization process of G_Y and D_Y is denoted as:

$$\min_{G_Y}\max_{D_Y}\mathcal{L}_{advY}(G_Y, D_Y)$$

(b) *Cycle-Consistent Losses*: The cycle-consistent loss ensures translations $G_X(X_{yng})$ and $G_Y(Y_{old})$ can be reverted to the X_{yng} and Y_{old} domains, respectively. It is given by

$$\mathcal{L}_{cyc}(G_X, G_Y) = \mathbb{E}_{y\sim p(Y_{old})}[\| G_Y(G_X(y)) - y \|_2] + \mathbb{E}_{x\sim p(X_{yng})}[\| G_X(G_Y(x)) - x \|_2]$$

(c) *Identity Losses*: The identity loss ensures that the transformation done by G_X and G_Y does not significantly alter input MRIs. It is given by:

$$\mathcal{L}_{idt}(G_X, G_Y) = \mathbb{E}_{y\sim p(Y_{old})}[\| (G_X(y)) - y \|_1] + \mathbb{E}_{x\sim p(X_{yng})}[\| (G_Y(x)) - x \|_1]$$

The overall objective function is the sum of the above three losses.

$$\mathcal{L}_{total} = \mathcal{L}_{adv}(G_X, D_X) + \mathcal{L}_{adv}(G_Y, D_Y) + \mathcal{L}_{cyc}(G_X, G_Y) + \mathcal{L}_{idt}(G_X, G_Y)$$

3. Results

3.1. Data Processing

All the data used in this study are 3D MRI scans obtained from the Alzheimer's Disease Neuroimaging Initiative (ADNI) Dataset [10]. This initiative aims to develop a multisite, longitudinal, prospective, naturalistic study of normal cognitive aging, mild cognitive impairment (MCI), and early Alzheimer's disease as a public-domain research resource to facilitate the scientific evaluation of neuroimaging and other biomarkers for the onset and progression of MCI and Alzheimer's disease. A total of 1152 images were used, with 384 images for each of the health states: Alzheimer's Disease (AD), Mild Cognitive Impairment (MCI), and Cognitively Normal (CN).

All volumetric data were skull-stripped and linearly registered to MNI 152 space using FSL-FLIRT and BET [28], [29]. I then normalized brain volumes using the Min-max norm by rescaling the resulting intensities to the range [−1, +1]. Such intensity pre-processing also helps alleviate potential intensity harmonization issues between datasets in a manner that creates no leakage. All processed brain volumes are cropped to the size of [256, 256, 160]. The grayscale channel is then added and transform the images to the size of [1, 256, 256, 160].

For the 2D model, the middle 60 axial slices are selected from each volume and cropped each slice to the size of [1, 256, 256]. For the 3D model, each brain volume is divided into 256 [1, 64, 64, 64] patches with a stride of [25, 25, 25]. During testing, the patches are assembled while applying Median Filtering of [3×3] to remove noises and preserve the edges of the generated image.

3.2. Baselines

2D conditional CycleGAN Network

This method is a trained 2D-based cycleGAN network. Translation from domains X to Y can be achieved by finding a latent representation that generates image X and then rendering this latent representation into style Y. The model is trained with cross-sectional data. The conditionals regarding the subject's age, sex, and AD status are involved in the image generation process. It receives and generates 2D scans only.

3D non-conditional CycleGAN Network

Like the proposed BrainSim, this method is a 3D-based bidirectional CycleGAN network that translates images back and forth between domains X and Y. However, this model contains a non-conditional generator. Thus, the condition of the designated health state and sex is not involved in the training process.

2D conditional GAN Network

This is a 2D conditional GAN model proposed by Xia et al [13]. The model contains a generator and a discriminator and synthesizes images conditioned on an individual's age and AD status. The model is trained using cross-sectional 2D images.

3.3. Implementation Details

To train the model, I selected images of the same age from each subject and paired them according to their health state before applying them to the model. Thus, the model is trained to generate aged and retrospective images within the same health state. For the testing of BrainSim, I paired images from the same subject but different ages. This reiterates my purpose that the model should be trained to generate images that are from the same subject as the input image. BrainSim was implemented using PyTorch [30]. It was trained for 384,000 iterations on one V100-SXM2-32GB GPU with a learning rate of $2 \times 10^{-4}$and a batch size of 10.

3.4. Quantitative Evaluation

3.4.1. Evaluation Metrics

To evaluate the quality of synthetically aged images, I used standard definitions of root mean squared error (RMSE), peak signal-to-noise ratio (PSNR), and structural similarity (SSIM) to evaluate the closeness of the predicted images to the ground truth [31].

PSNR is the quantity measured as the ratio between the power of the signal noise and a signal's maximum power [32]. It is commonly used to measure the quality of images in various applications involving compression and reconstruction. The higher the PSNR, the higher the quality of the extracted image.

SSIM is used to quantify the structural similarity between two images [33]. It is based on luminance, contrast, and changes in structural information. In contrast to PSE and PSNR, SSIM gives perception and saliency-based errors [34]. Thus, it is designed to model the human visual system more closely than PSNR and MSE, making it more aligned with human perception of image quality.

3.4.2. Result Analysis

Table 1. Quantitative evaluation of 2D conditional, Xia et al., 3D non-conditional, and BrainSim for several metrics

	AD			MCI			CN		
	PSNR	SSIM	RMSE	PSNR	SSIM	RMSE	PSNR	SSIM	RMSE
2D cond.	16.463	0.602	0.177	14.225	0.521	0.245	13.767	0.481	0.237
Xia et al.	17.698	0.563	0.122	17.618	0.542	0.101	18.719	0.760	0.134
3D non-cond.	18.250	0.622	0.132	17.912	0.576	0.127	18.072	0.575	0.125
BrainSim	**24.734**	**0.865**	**0.058**	**23.285**	**0.852**	**0.069**	**24.940**	**0.799**	**0.111**

	AD			MCI			CN		
	PSNR	SSIM	RMSE	PSNR	SSIM	RMSE	PSNR	SSIM	RMSE
2D cond.	16.541	0.579	0.174	14.564	0.547	0.239	14.136	0.414	0.224
3D non-cond.	18.633	0.583	0.117	18.125	0.562	0.124	18.743	0.443	0.116
BrainSim	**25.902**	**0.831**	**0.051**	**25.553**	**0.877**	**0.053**	**24.269**	**0.899**	**0.061**

The upper one measures the accuracy of aged brain MRI generation; the lower one measures the accuracy of retrospective brain MRI generation.

The quantitative results are shown in Table 1. The evaluation metrics employed are the PSNR, which measures the quality of the reconstruction by quantifying the ratio between the maximum possible power of a signal and the power of corrupting noise that affects the fidelity of its representative; SSIM, which measures the similarity between two images based on three components: luminance similarity, contrast similarity, and structure similarity; and RMSE, measuring the average deviation of predicted values from the actual values.

Compared to the model proposed by Xia et al., BrainSim demonstrated an average 6.308 increase in PSNR. This suggests that when trained with limited MRI slices, BrainSim performs with a higher accuracy, which can be attributed to the cycle-GAN architecture it uses.

The change from a 2D to a 3D-based network shows a significant increase in the performance of the model. For the aged brain simulation, an average increase of 9.501dB in PSNR value is observed across all health states. In addition, the SSIM value experienced an average increase of 0.396 in SSIM, while the mean RMSE values had a 0.140 decrease. Simultaneously, the retrospective brain simulation resulted in a 10.161 dB increase in PSNR, a 0.356 increase in SSIM, and a 0.157 decline in RMSE.

It is thus indicated that BrainSim has a superior performance across all three health states in both aged and retrospective brain simulation. More importantly, the retrospective brain generation processes yielded an accuracy that is 0.922dB SSIM higher than that of the aging process.

3.5. Qualitative Evaluation

3.5.1. Evaluation Metrics

To evaluate the performance of the models qualitatively, error maps are used to visually represent the discrepancies and differences between the generated images and the ground truths. Specifically, these error maps are generated by computing the pixel-wise differences between the generated image and the target image.

I also used a Global-local Transformer-based age-predicting model to predict the actual age of the MRI scans [35]. I trained the model with 3D images from the ADNI dataset. The trained age prediction model yielded a mean absolute error (MAE) of 3.1 years.

3.5.2. Result Analysis

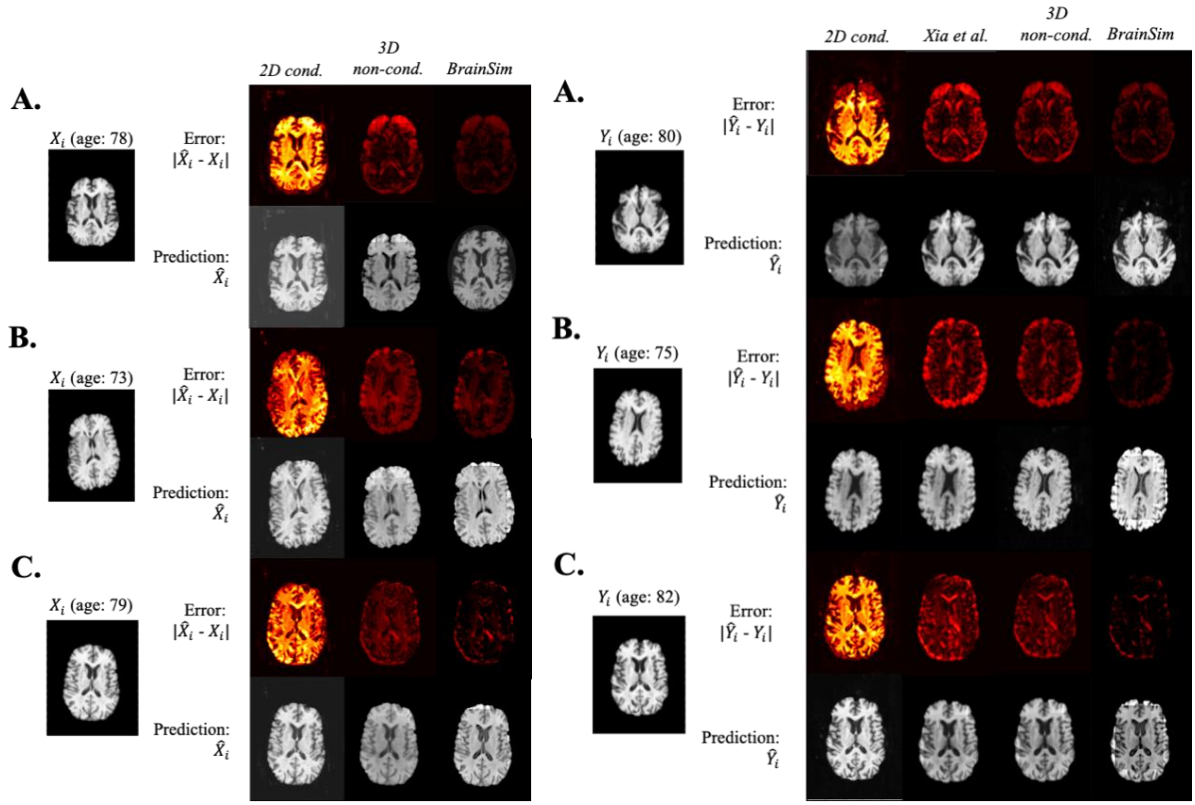

Figure 4. Examples results of (A) AD; (B) MCI; and (C) CN image generation

Results of both brain aging (left) and retrospecting (right) are shown for each health state. I predict output $\hat{Y}_i$ from input X_i and output $\hat{X}_i$ from input Y_i using baseline models and my method. Errors between the outputs and the ground-truths as $|\hat{X}_i - X_i|$ and $|\hat{Y}_i - Y_i|$ are also shown. It can be observed that BrainSim achieves the most accurate results outperforming the baseline models. For more details see text.

As demonstrated in Fig.4, the best results are achieved by the 3D conditional model, BrainSim, where the least error between $\hat{X}_i - X_i$ and $\hat{Y}_i - Y_i$ is observed. The 2D conditional model produced the poorest output images, with observable structural differences from ground truth, indicating loss of subject identity. It is also noticeable that the brain ventricle is enlarged in BrainSim results and the values of $|\hat{X}_i - X_i|$ and $|\hat{Y}_i - Y_i|$ are reduced, which is consistent with the accepted fact that the ventricle increases during the aging process.

Furthermore, the result of the same AD subject at different target ages is shown in Fig. 5. The brain generations from age 58 to 98 are shown with a 5-year increment. It is obvious that as the age difference between the target age and the original age increases, more observable errors and discrepancies between the generated image and the ground truth start to exist. This observation is consistent with the prior findings that AD progression can be indicated by the chronicle-changing process of the brain over a period of time [4]. I then used f_{pred} to estimate the age of these synthetic images. On average across 300 samples of AD, MCI, and CN images, synthetic AD images are 4.5 ± 2.0 years older than the target age, whereas synthetic MCI and CN images are 1.9 ± 3.1 years and 1.5 ± 2.4 years older than the target

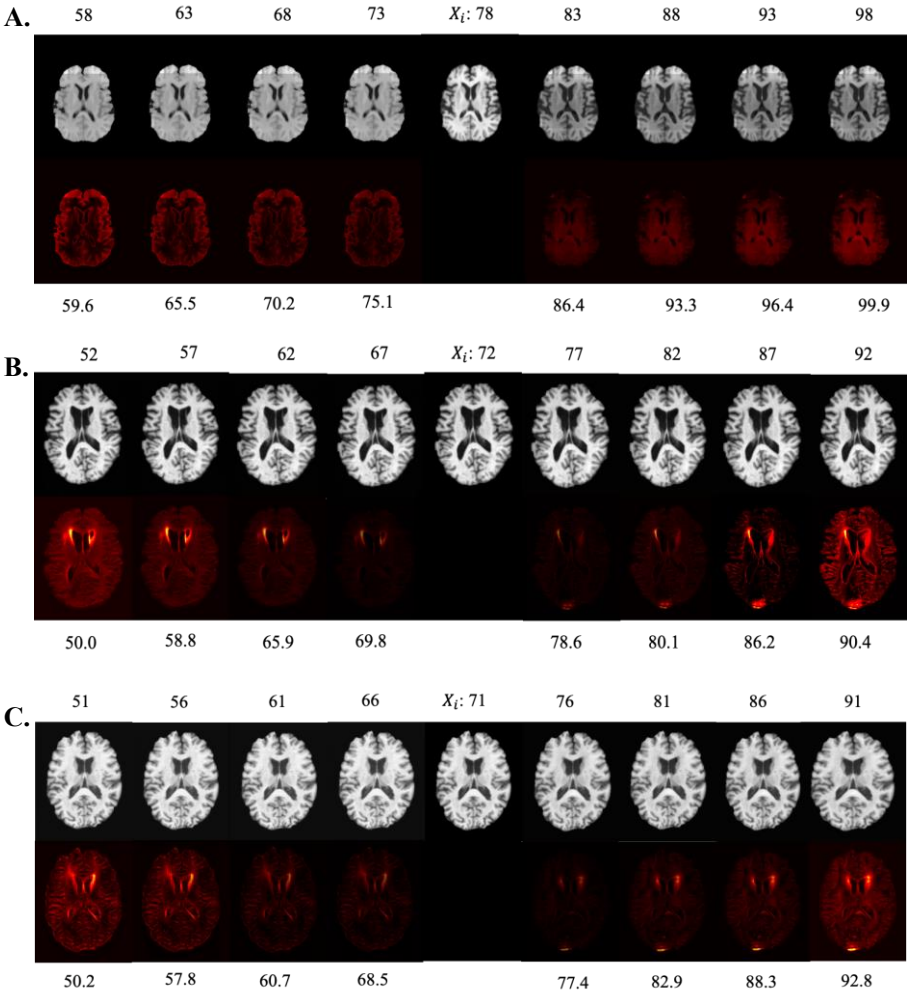

Figure 5. Brain aging and retrospecting progression for (A)AD subject X_i (at age 78); (B) MCI subject X_i(at age 72); (C) CN subject X_i(at age 71)

The aged and retrospective images, $\widehat{Y}_i$ and $\widehat{X}_i$, respectively, are generated are compared. The differences between generated images and ground truths, $|\widehat{X}_i - X_i|$ and $|\widehat{Y}_i - Y_i|$, are visualized along with the simulations $\widehat{Y}_i$ and $\widehat{X}_i$. I also show the predicted (apparent) ages of X_i as obtained by the pre-trained age predictor (below the generated images).

age, respectively. These observations are consistent with previous studies that AD accelerates brain aging [10]. A larger discrepancy between the target and predicted ages of the brain of AD patients are observed as the target age becomes larger (it is important to know that the maximum age of the age predictor is set to be 100.0).

I also observe that the gray/white matter contrast decreases as age increases in the generated images, which is consistent with existing findings [36]. In addition, enlarging ventricle volume is also observed from the generated AD images, which is consistent with current findings [37].

4. Discussion

BrainSim, as presented in this paper, is a novel method for generating aged and retrospective subject-specific brain MRI scans without using longitudinal data. Utilizing a double-sided conditional U-Net architecture with embedded age, health state, and sex information, BrainSim effectively simulates brain images subjected to subject-specific clinical variables. The cycleGAN-based architecture, along with age-modulated and self-reconstruction losses, ensures that the generated images maintain subject identity and consistency throughout the generation process.

The effectiveness of BrainSim was demonstrated through evaluations on the ADNI dataset, showing its capability to produce realistic images conditioned on age, sex, and health state. The qualitative and quantitative results indicate superior performance compared to benchmarks, thus underscoring BrainSim's potential to address existing challenges in longitudinal MRI studies by imputing missing data and ensuring study continuity.

Table 2. Feature Comparison to existing deep learning-based MRI generation models (Dep-GAN, Xia et al., and DaniNet)

	DEP-GAN	Xia et al.	DaniNet	BrainSim
Rejuvenation	×	×	×	√
3D MRI Images	×	×	×	√
Longitudinal MRI-Free	√	√	×	√
Health-conditioned	×	√	√	√
Sex-conditioned	×	×	×	√

The five features being compared are brain MRI rejuvenation capability, the dimension of the model, the need of longitudinal MRIs, and whether the image generation processed are health and sex-conditioned.

As suggested by table 2, compared with existing studies, BrainSim is unique due to its bidirectional architecture and sex-included image generation algorithms [14], [23], [41]. A study by Aggarwal et al. suggests that the clinical presentation, cognitive testing profiles, and biomarker profiles of AD all differ by sex [38]. Thus, the overlook of sex as a variable in image generation is likely to be one of the major sources of error in previous models [14]. The high performance of BrainSim can thus be partly attributed to the sex-oriented image generation algorithm it obtains.

As one of the few 3D image synthesis models, BrainSim outperforms other 2D networks by preserving more details and predicting structural changes more accurately in a 3D space. Since 3D MRI can provide better image quality, especially for complex anatomical structures, it is more well-suited for advanced post-processing techniques such as 3D reconstruction. The implementation of a 3D network of BrainSim thus further improves the accuracy of the generation and increases the performance of the model. In addition, the use of 3D image segmentation also reduces the potential error of miss-matching slices, which is found in multiple models using 2D image slices [13]. Despite posing challenges to the device and the length of training, the implementation of a 3D network can greatly increase the precision of the generated image and therefore increase its chance to be used in clinical and research industries.

4.1. Potential applications

BrainSim has several potential applications. BrainSim can allow researchers to impute the missing MRI data of a patient at any time point since missing data due to patient dropout and poor-quality scans are common challenges in longitudinal MRI studies. In addition, BrainSim is proven to have sufficiently understood the structural changes in AD patients, as discussed in section 3.4.2. This suggests that BrainSim has huge potential for clinical use, allowing further clinical analysis of aging patterns and possibly fostering studies into neurodegenerative diseases. Lastly, I have successfully extended the cycleGAN structure so that it can be applied in the field of medical image processing

and generation. BrainSim's major pipeline can be employed in the image generation of other types (i.e. CT, PET, SPECT) and body parts (i.e. blood vessels, abdomen, lymph nodes).

4.2. Limitations and avenues for improvement

While I employed various loss functions to maintain the subject identity in generated images, it is important to recognize that this doesn't guarantee the preservation of an individual's identity. Further analysis of new loss functions and mechanisms could potentially enhance identity preservation. Unfortunately, due to the limited accessible data on different variables related to identity, pathology, and demographics, the level of preservation of identity can only be approximated.

In this paper, I use a simple way to encode both age and AD status conditions into the image generation network. However, the use of further clinical information to reflect health status can be of benefit as the classification of MCI is challenging and equivocal. Additional clinical variables such as genotypes can also be incorporated into the model for better image generation and disease progression prediction. While researchers are experimenting with new techniques to incorporate these variables into the process of image generation, their utility in integrating clinical variables with imaging data is still under investigation [39], [40].

Furthermore, in this paper, I focus on the use of cross-sectional data to train a model to predict aged and retrospective brain images. If longitudinal MRI data are available, model performance could be further improved by implementing supervised losses and transforming the model into a semi-supervised learning model.

5. Conclusion

This paper presents a method that learns to simulate both aged and retrospective subject-specific brain MRI scans without longitudinal data. It relies on two conditional U-Net generators to generate the images and two Multilayer Discriminators. The generator captures the joint distribution of brain images and clinical variables, i.e. age, health state (AD status), and sex. The proposed cycleGAN-based network allows the simultaneous generation of aged and retrospective brain MRIs. BrainSim consists of an embedding mechanism to encode the information of age, health state, and sex into the network, and age-modulated and self-reconstruction losses to preserve subject identity. I also use cycle-consistent loss to maintain the consistency of the generators.

I present qualitative results showing that my method can generate consistent and realistic images conditioned on the target age and health state. I evaluate with longitudinal data from ADNI for image quality and age accuracy. I demonstrate on ADNI that BrainSim outperforms benchmarks both qualitatively and quantitatively and, via a series of ablations, illustrate the importance of each design decision. BrainSim, therefore, has the potential for clinical and research applications.

References

[1] F. Alshehri, "Integrated virtual screening, molecular modeling and machine learning approaches revealed potential natural inhibitors for epilepsy," *Saudi Pharm. J.*, vol. 31, no. 12, p. 101835, Dec. 2023, doi: 10.1016/j.jsps.2023.101835.

[2] J. Lam, J. Lee, C. Y. Liu, A. M. Lozano, and D. J. Lee, "Deep Brain Stimulation for Alzheimer's Disease: Tackling Circuit Dysfunction," *Neuromodulation Technol. Neural Interface*, vol. 24, no. 2, pp. 171 – 186, Feb. 2021, doi: 10.1111/ner.13305.

[3] J. Rasmussen and H. Langerman, "Alzheimer's Disease – Why We Need Early Diagnosis," *Degener. Neurol. Neuromuscul. Dis.*, vol. Volume 9, pp. 123–130, Dec. 2019, doi: 10.2147/DNND.S228939.

[4] J. H. Cole, R. E. Marioni, S. E. Harris, and I. J. Deary, "Brain age and other bodily 'ages': implications for neuropsychiatry," *Mol. Psychiatry*, vol. 24, no. 2, pp. 266 – 281, Feb. 2019, doi: 10.1038/s41380 – 018 - 0098 - 1.

[5] L. Chouliaras and J. T. O'Brien, "The use of neuroimaging techniques in the early and differential diagnosis of dementia," *Mol. Psychiatry*, Aug. 2023, doi: 10.1038/s41380 - 023 - 02215 - 8.

[6] S. Aramadaka *et al.*, "Neuroimaging in Alzheimer's Disease for Early Diagnosis: A Comprehensive Review," *Cureus*, May 2023, doi: 10.7759/cureus.38544.

[7] X. Song *et al.*, "Strengths and challenges of longitudinal non-human primate neuroimaging," *NeuroImage*, vol. 236, p. 118009, Aug. 2021, doi: 10.1016/j.neuroimage.2021.118009.

[8] Y. Wu, Q. Liu, Y. Qiu, and L. Xie, "Deep learning prediction of chemical-induced dose-dependent and context-specific multiplex phenotype responses and its application to personalized alzheimer's disease drug repurposing," *PLOS Comput. Biol.*, vol. 18, no. 8, p. e1010367, Aug. 2022, doi: 10.1371/journal.pcbi.1010367.

[9] P. -L. Kuo *et al.*, "A roadmap to build a phenotypic metric of ageing: insights from the Baltimore Longitudinal Study of Aging," *J. Intern. Med.*, vol. 287, no. 4, pp. 373 – 394, Apr. 2020, doi: 10.1111/joim.13024.

[10] R. C. Petersen *et al.*, "Alzheimer's Disease Neuroimaging Initiative (ADNI): Clinical characterization," *Neurology*, vol. 74, no. 3, pp. 201 – 209, Jan. 2010, doi: 10.1212/WNL.0b013e3181cb3e25.

[11] M. Hajij, G. Zamzmi, R. Paul, and L. Thukar, "Normalizing Flow for Synthetic Medical Images Generation," in *2022 IEEE Healthcare Innovations and Point of Care Technologies (HI-POCT)*, Houston, TX, USA: IEEE, Mar. 2022, pp. 46 – 49. doi: 10.1109/HI-POCT54491.2022.9744072.

[12] S. Pal, S. Dutta, and R. Maitra, "Fast matrix-free methods for model-based personalized synthetic MR imaging." arXiv, Aug. 24, 2023. Accessed: Jun. 15, 2024. [Online]. Available: http://arxiv.org/abs/2103.01532

[13] T. Xia, A. Chartsias, C. Wang, and S. A. Tsaftaris, "Learning to synthesise the ageing brain without longitudinal data," *Med. Image Anal.*, vol. 73, p. 102169, Oct. 2021, doi: 10.1016/j.media.2021.102169.

[14] D. Ravi, D. C. Alexander, and N. P. Oxtoby, "Degenerative Adversarial NeuroImage Nets: Generating Images that Mimic Disease Progression." arXiv, Aug. 30, 2019. Accessed: Mar. 14, 2024. [Online]. Available: http://arxiv.org/abs/1907.02787.

[15] T. Wang *et al.*, "A review on medical imaging synthesis using deep learning and its clinical applications," *J. Appl. Clin. Med. Phys.*, vol. 22, no. 1, pp. 11 – 36, Jan. 2021, doi: 10.1002/acm2.13121.

[16] Y. Zhang, M. Brady, and S. Smith, "Segmentation of brain MR images through a hidden Markov random field model and the expectation-maximization algorithm," *IEEE Trans. Med. Imaging*, vol. 20, no. 1, pp. 45 – 57, Jan. 2001, doi: 10.1109/42.906424.

[17] J. Pegueroles *et al.*, "Longitudinal brain structural changes in preclinical Alzheimer's disease," *Alzheimers Dement.*, vol. 13, no. 5, pp. 499 – 509, May 2017, doi: 10.1016/j.jalz.2016.08.010.

[18] A. Machado *et al.*, "The cholinergic system in subtypes of Alzheimer's disease: an in vivo longitudinal MRI study," *Alzheimers Res. Ther.*, vol. 12, no. 1, p. 51, Dec. 2020, doi: 10.1186/s13195 - 020 - 00620 - 7.

[19] J. Zhang, M. Liu, Le An, Y. Gao, and D. Shen, "Alzheimer's Disease Diagnosis Using Landmark-Based Features from Longitudinal Structural MR Images," *IEEE J. Biomed. Health Inform.*, vol. 21, no. 6, pp. 1607 – 1616, Nov. 2017, doi: 10.1109/JBHI.2017.2704614.

[20] C. Platero, M. C. Tobar, and for the Alzheimer's Disease Neuroimaging Initiative, "Predicting Alzheimer's conversion in mild cognitive impairment patients using longitudinal neuroimaging and clinical markers," *Brain Imaging Behav.*, vol. 15, no. 4, pp. 1728–1738, Aug. 2021, doi: 10.1007/s11682 -020 - 00366 - 8.

[21] D. Milana, "Deep generative models for predicting Alzheimer's disease progression from MRI data.," *Politec. MILANO Sch. Ind. Inf. Eng.*, 2017.

[22] N. Pawlowski, D. C. Castro, and B. Glocker, "Deep Structural Causal Models for Tractable Counterfactual Inference." arXiv, Oct. 22, 2020. Accessed: Mar. 17, 2024. [Online]. Available: http://arxiv.org/abs/2006.06485.

[23] M. F. Rachmadi, M. Del C. Valdés-Hernández, S. Makin, J. M. Wardlaw, and T. Komura, "Predicting the Evolution of White Matter Hyperintensities in Brain MRI Using Generative Adversarial Networks and Irregularity Map," in *Medical Image Computing and Computer Assisted Intervention – MICCAI 2019*, vol. 11766, D. Shen, T. Liu, T. M. Peters, L. H. Staib, C. Essert, S. Zhou, P.-T. Yap, and A. Khan, Eds., in Lecture Notes in Computer Science, vol. 11766., Cham: Springer International Publishing, 2019, pp. 146–154. doi: 10.1007/978 – 3 - 030 - 32248 - 9_17.

[24] V. Wegmayr, M. Hörold, and J. M. Buhmann, "Generative Aging of Brain MR-Images and Prediction of Alzheimer Progression," in *Pattern Recognition*, vol. 11824, G. A. Fink, S. Frintrop, and X. Jiang, Eds., in Lecture Notes in Computer Science, vol. 11824. , Cham: Springer International Publishing, 2019, pp. 247–260. doi: 10.1007/978-3-030-33676-9_17.

[25] Q. Zhao, E. Adeli, N. Honnorat, T. Leng, and K. M. Pohl, "Variational AutoEncoder for Regression: Application to Brain Aging Analysis." arXiv, Jul. 11, 2019. Accessed: Mar. 14, 2024. [Online]. Available: http://arxiv.org/abs/1904.05948.

[26] O. Ronneberger, P. Fischer, and T. Brox, "U-Net: Convolutional Networks for Biomedical Image Segmentation," 2015, doi: 10.48550/ARXIV.1505.04597.

[27] B. Xu, N. Wang, T. Chen, and M. Li, "Empirical Evaluation of Rectified Activations in Convolutional Network." arXiv, Nov. 27, 2015. Accessed: Mar. 16, 2024. [Online]. Available: http://arxiv.org/abs/1505.00853.

[28] S. M. Smith, "Fast robust automated brain extraction.," *Hum. Brain Mapp.*, vol. 17(3):143-155, Nov. 2002.

[29] M. W. Woolrich *et al.*, "Bayesian analysis of neuroimaging data in FSL," *NeuroImage*, vol. 45, no. 1, pp. S173–S186, Mar. 2009, doi: 10.1016/j.neuroimage.2008.10.055.

[30] A. Paszke *et al.*, "PyTorch: An Imperative Style, High-Performance Deep Learning Library," 2019, doi: 10.48550/ARXIV.1912.01703.

[31] Z. Wang, E. P. Simoncelli, and A. C. Bovik, "Multiscale structural similarity for image quality assessment," in *The Thrity-Seventh Asilomar Conference on Signals, Systems & Computers, 2003*, Pacific Grove, CA, USA: IEEE, 2003, pp. 1398 – 1402. doi: 10.1109/ACSSC.2003.1292216.

[32] D. Sethi, S. Bharti, and C. Prakash, "A comprehensive survey on gait analysis: History, parameters, approaches, pose estimation, and future work," *Artif. Intell. Med.*, vol. 129, p. 102314, Jul. 2022, doi: 10.1016/j.artmed.2022.102314.

[33] Z. Wang, A. C. Bovik, H. R. Sheikh, and E. P. Simoncelli, "Image Quality Assessment: From Error Visibility to Structural Similarity," *IEEE Trans. Image Process.*, vol. 13, no. 4, pp. 600–612, Apr. 2004, doi: 10.1109/TIP.2003.819861.

[34] J. Guerreiro, P. Tomás, N. Garcia, and H. Aidos, "Super-resolution of magnetic resonance images using Generative Adversarial Networks," *Comput. Med. Imaging Graph.*, vol. 108, p. 102280, Sep. 2023, doi: 10.1016/j.compmedimag.2023.102280.

[35] S. He, P. E. Grant, and Y. Ou, "Global-Local Transformer for Brain Age Estimation," *IEEE Trans. Med. Imaging*, vol. 41, no. 1, pp. 213 – 224, Jan. 2022, doi: 10.1109/TMI. 2021. 3108910.

[36] L. T. Westlye *et al.*, "Increased sensitivity to effects of normal aging and Alzheimer's disease on cortical thickness by adjustment for local variability in gray/white contrast: A multi-sample MRI study," *NeuroImage*, vol. 47, no. 4, pp. 1545 – 1557, Oct. 2009, doi: 10.1016/j.neuroimage.2009.05.084.

[37] L. Ferrarini, W. M. Palm, H. Olofsen, M. A. Van Buchem, J. H. C. Reiber, and F. Admiraal-Behloul, "Shape differences of the brain ventricles in Alzheimer's disease," *NeuroImage*, vol. 32, no. 3, pp. 1060 – 1069, Sep. 2006, doi: 10.1016/j.neuroimage.2006.05.048.

[38] N. T. Aggarwal and M. M. Mielke, "Sex Differences in Alzheimer's Disease," *Neurol. Clin.*, vol. 41, no. 2, pp. 343 – 358, May 2023, doi: 10.1016/j.ncl.2023.01.001.

[39] X. Huang and S. Belongie, "Arbitrary Style Transfer in Real-time with Adaptive Instance Normalization," 2017, doi: 10.48550/ARXIV.1703.06868.

[40] E. Perez, F. Strub, H. De Vries, V. Dumoulin, and A. Courville, "FiLM: Visual Reasoning with a General Conditioning Layer," *Proc. AAAI Conf. Artif. Intell.*, vol. 32, no. 1, Apr. 2018, doi: 10.1609/aaai. v32i1. 11671.

[41] Z. Li, Q. Zheng, B. Shi, G. Pan, and X. Jiang, "DANI-Net: Uncalibrated Photometric Stereo by Differentiable Shadow Handling, Anisotropic Reflectance Modeling, and Neural Inverse Rendering," Mar. 28, 2023, *arXiv*: arXiv:2303.15101. Accessed: Jul. 26, 2024. [Online]. Available: http: //arxiv.org/abs/2303. 15101.